Desensitization Contributes to the Synaptic Response of Gain-of-Function Mutants of the Muscle Nicotinic Receptor

Sergio Elenes, Ying Ni, Gisela D. Cymes, and Claudio Grosman

Department of Molecular and Integrative Physiology, Center for Biophysics and Computational Biology, and Neuroscience Program, University of Illinois at Urbana-Champaign, Urbana, IL 61801

Although the muscle nicotinic receptor (AChR) desensitizes almost completely in the steady presence of high concentrations of acetylcholine (ACh), it is well established that AChRs do not accumulate in desensitized states under normal physiological conditions of neurotransmitter release and clearance. Quantitative considerations in the framework of plausible kinetic schemes, however, lead us to predict that mutations that speed up channel opening, slow down channel closure, and/or slow down the dissociation of neurotransmitter (i.e., gain-of-function mutations) increase the extent to which AChRs desensitize upon ACh removal. In this paper, we confirm this prediction by applying high-frequency trains of brief (~1 ms) ACh pulses to outside-out membrane patches expressing either lab-engineered or naturally occurring (disease-causing) gain-of-function mutants. Entry into desensitization was evident in our experiments as a frequency-dependent depression in the peak value of succesive macroscopic current responses, in a manner that is remarkably consistent with the theoretical expectation. We conclude that the comparatively small depression of the macroscopic currents observed upon repetitive stimulation of the wild-type AChR is due, not to desensitization being exceedingly slow but, rather, to the particular balance between gating, entry into desensitization, and ACh dissociation rate constants. Disruption of this fine balance by, for example, mutations can lead to enhanced desensitization even if the kinetics of entry into, and recovery from, desensitization themselves are not affected. It follows that accounting for the (usually overlooked) desensitization phenomenon is essential for the correct interpretation of mutagenesis-driven structure–function relationships and for the understanding of pathological synaptic transmission at the vertebrate neuromuscular junction.

INTRODUCTION

As is the case for most other neurotransmitter-gated ion channels, the desensitized state of the muscle nicotinic acetylcholine receptor (AChR) is the most stable allosteric form for the fully liganded (i.e., diliganded) receptor (Katz and Thesleff, 1957; Karlin, 1967; Edelstein and Changeux, 1998). This "state" comprises a number of kinetically distinguishable protein conformations (Heidmann and Changeux, 1980; Neubig and Cohen, 1980; Reitstetter et al., 1999; Elenes and Auerbach, 2002) in which the channel is ion impermeable (like in the closed state), and ACh is bound with high affinity (like in the open state). Indeed, when AChRs are exposed to a step change in ACh concentration from zero to saturating, the increase in the current is only transient, reflecting the initial channel opening followed by entry into the more stable, desensitized state (Katz and Thesleff, 1957; Magleby and Pallotta, 1981; Cachelin and Colquhoun, 1989; Dilger and Liu, 1992; Franke et al., 1993). Thus, under the steady presence of saturating concentrations of ACh, nearly all AChRs are desensitized (Sakmann et al., 1980). However, the particular time course of ACh in the synaptic cleft, combined with the particular kinetics of the wild-type AChR, results in the AChR not normally accumulating in desensitized states.

It is probably a reasonable approximation to assume that, during normal neuromuscular transmission, AChRs are alternatively exposed to millimolar and nearly zero levels of ACh as cycles of neurotransmitter release and removal take place. Typically, each "pulse" of millimolar ACh lasts only a few hundred microseconds (Magleby and Stevens, 1972; Wathey et al., 1979; Land et al., 1981; Dudel et al., 1999), whereas the duration of the intervening, interpulse intervals is ~10 ms or longer (from the notion that, in mammals, the firing frequency of fast motor units rarely exceeds ~100 Hz; Hennig and Lømo, 1985). Although each pulse of millimolar ACh is only a few hundred microseconds long, most AChRs are expected to be open and bound to two molecules of ACh by the end of the pulse. Because diliganded wild-type AChRs desensitize relatively slowly, though, entry into desensitization (and the accompanying current decay) is minimal during ACh pulses.

During interpulse intervals, however, the endplate current through wild-type AChRs decays completely,

Correspondence to Claudio Grosman: grosman@life.uiuc.edu

S. Elenes's present address is University Center for Biomedical Research, University of Colima, Colima, 28045, Mexico.

Abbreviations used in this paper: ACh, acetylcholine; AChE, acetylcholinesterase; AChR, ACh receptor.

J. Gen. Physiol. © The Rockefeller University Press $8.00
Volume 128 Number 5 November 2006 615–627
http://www.jgp.org/cgi/doi/10.1085/jgp.200609570

following a nearly monoexponential time course (Magleby and Stevens, 1972). Inspection of the kinetic scheme in Fig. 1 suggests that the kinetics of this decay depend on the rate constants of interconversion among the different diliganded conformations, and on the rate constants of neurotransmitter dissociation from them (the concentration of neurotransmitter in the cleft becomes so low that its reassociation can be neglected). In the particular case of the muscle AChR, reopening of diliganded desensitized receptors ($DA_2 \rightarrow OA_2$ or $DA_2 \rightarrow CA_2 \rightarrow OA_2$; Fig. 1) is much slower than ACh dissociation from them ($DA_2 \rightarrow DA$; Franke et al., 1993). As a result, diliganded receptors oscillate a few times between the open and closed conformations until the desensitized state is entered (most frequently through an $OA_2 \rightarrow DA_2$ transition; Auerbach and Akk, 1998) or ACh unbinds from the closed or the open states (followed by closure; Grosman and Auerbach, 2001). Indeed, using the scheme in Fig. 1, and under the condition that the probability of the channel being open while fluctuating between the OA_2 and CA_2 states is close to unity (which is the case for the wild-type and mutant AChRs studied here), it can be calculated that the time course of the current decay upon stepping the ACh concentration to zero is dominated by a single exponential component, in agreement with experimental observations (Fig. 2 A). Further, it can be shown that the time constant of this component (the exact value of which is given by one of the eigenvalues of the minus Q matrix corresponding to the scheme in Fig. 1) is very well approximated by an extremely simple analytical expression (Grosman and Auerbach, 2001; see red arrows in Fig. 1):

$$\tau_{deactivation} \cong \frac{1}{D_+ + 2j_- + \frac{\alpha_2 2k_-}{\beta_2 + 2k_-}}. \quad (1)$$

This time constant is usually referred to as the deactivation time constant and, in the particular context of the neuromuscular junction, is also referred to as the time constant of the endplate current decay. Interestingly, this macroscopic quantity can also be obtained from single-channel recordings performed at very low concentrations of neurotransmitter, as the time constant of the slowest component of the closed≡open burst length distribution (Fig. 2 B and Fig. 3; Grosman and Auerbach, 2001; for the underlying theory, see Colquhoun et al., 1997; Wyllie et al., 1998).

The relative contributions of entry into desensitization, ACh dissociation from the closed state, and ACh dissociation from the open state (followed by closure) to the current decay upon ACh removal depend, as expected, on the particular values of the rate constants in the pertinent kinetic scheme. In the framework of the model in Fig. 1, the probability of the AChR entering

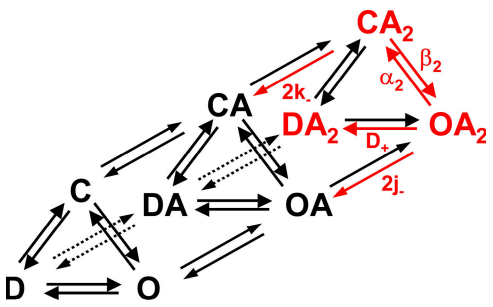

Figure 1. An allosteric reaction mechanism for the muscle AChR. C, O, and D denote the closed, open, and desensitized conformations of the channel, whereas A denotes a molecule of ACh. For simplicity, only one of the (probably several) desensitized conformations is included in the model. Also, the two neurotransmitter binding sites are assumed to be functionally equivalent and independent and, therefore, the two possible monoliganded configurations are considered to be functionally indistinguishable. These simplifications have no consequences on the interpretation of our data. The red arrows indicate the rate constants that, according to Eq. 1, determine the kinetics of the macroscopic current decay upon stepping the concentration of ACh from saturating to zero (i.e., during channel deactivation).

a desensitized conformation during deactivation can be calculated as

$$\text{Probability of desensitizing} = \frac{D_+}{D_+ + 2j_- + \frac{\alpha_2 2k_-}{\beta_2 + 2k_-}}. \quad (2)$$

Thus, using Eq. 2 and wild-type values for the adult form of the receptor (i.e., $D_+ = 25\ s^{-1}$, $k_- = 20{,}000\ s^{-1}$, $j_- = 12\ s^{-1}$, $\beta_2 = 50{,}000\ s^{-1}$, $\alpha_2 = 2{,}000\ s^{-1}$), it can be calculated that the $\alpha_2 2k_-/(\beta_2 + 2k_-)$ term in Eq. 2 is so large ($\sim 900\ s^{-1}$) that the extent of entry into desensitization during channel deactivation is small (~ 0.03 after each individual ACh pulse). Similarly, the contribution of ACh dissociation from the open state to the deactivation time course can be calculated to be small in the wild-type AChR. This is entirely consistent with the well-established notion that, in normal endplates, it is the ACh dissociation from the closed state that terminates most bursts of diliganded closed≡open isomerizations and, therefore, that the deactivation time constant is, roughly, the reciprocal of $\alpha_2 2k_-/(\beta_2 + 2k_-)$ (Colquhoun and Hawkes, 1982).

However, the contribution of desensitization to channel deactivation is expected to increase as the $\alpha_2 2k_-/(\beta_2 + 2k_-)$ term in Eq. 2 is reduced by, say, mutations (Grosman and Auerbach, 2001). That is, not only changes in the kinetics of entry into desensitization, but also changes in the kinetics of gating and neurotransmitter dissociation are expected to affect the contribution of desensitization to the current decay that occurs upon stepping the ACh concentration to zero. Many mutations,

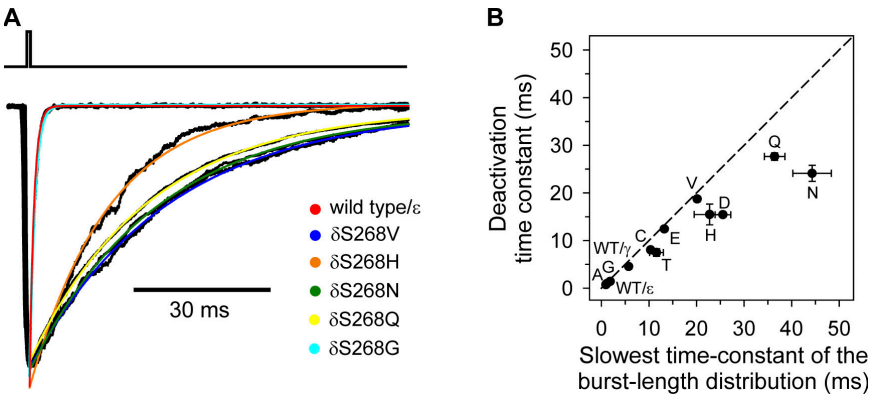

Figure 2. AChR deactivation. (A) The kinetics of deactivation were estimated by exposing outside-out patches (−80 mV) to ∼1-ms, 100 μM ACh pulses. Each plotted trace is the average response of a patch to 10 such pulses applied as a ≤1-Hz train. For clarity, only the responses of some of the studied constructs are shown. All traces were aligned and normalized for easier comparison, and their decaying phases were fitted (least-squares method) from the peak of the current until the end of the transient with single exponential components. The deactivation time constants, averaged over a number of patches per construct, are listed in Table I. (B) Correlation between the (macroscopic) deactivation time constants and the (single-channel) time constants of the slowest component of burst length distributions. It can be shown that for a kinetic scheme like that in Fig. 1 and rate constants like those of the constructs studied here, these two quantities coincide (Colquhoun et al., 1997; Wyllie et al., 1998). For all constructs, single-channel measurements were performed in the cell-attached configuration. In addition, for the Asp, Asn, and Gln mutants, these measurements were also done in the outside-out configuration, and the results were indistinguishable from those obtained in cell-attached experiments. Hence, the reason for the deviation of these mutants' data points from the expected straight line of unity slope (dashed line) remains unclear. Error bars are standard errors.

both lab-engineered and naturally occurring, decrease this term. These are usually referred to as gain-of-function mutations because they slow down the time course of deactivation (i.e., they increase $\tau_{deactivation}$; see Eq. 1). Gratifyingly, the prediction of an increased extent of desensitization during deactivation, as a result of gain-of-function mutations, was fully borne out by our experimental observations.

MATERIALS AND METHODS

Heterologous Expression and Mutagenesis

HEK-293 cells were transiently transfected with mouse muscle AChR complementary DNA (provided by S.M. Sine, Mayo Clinic, Rochester, MN), using a calcium-phosphate precipitation method (Purohit and Grosman, 2006). Mutations were engineered with a QuikChange site-directed mutagenesis kit (Stratagene) and were confirmed by dideoxy sequencing. All mutant δ subunits were coexpressed with wild-type α, β, and ε AChR subunits. For all macroscopic current recording experiments, cells were grown on poly-L-lysine–coated coverslips, whereas, for single-channel recordings, cells were grown on either coated coverslips or directly onto 35-mm plastic culture dishes.

Solution Exchange and Patch-Clamp Recordings

Step changes in the ACh concentration applied to outside-out patches were achieved by the rapid switching of two solutions flowing from either barrel of a piece of theta-type capillary glass tubing (Hilgenberg), essentially as described by Jonas (Jonas, 1995). The theta tube was mounted on a piezo-electric device (Burleigh-LSS-3100; Exfo), the movement of which was controlled by a computer using a Digidata 1322A interface (Molecular Devices) and pClamp 9.0 software (Molecular Devices). To minimize distortions in the time course of the solution exchange, the computer-generated rectangular waveforms (brief pulses, long pulses, and trains of brief pulses) were low-pass filtered (f_c = 125–150 Hz) before being applied to the piezo-electric device. The recording chamber (designed in-house) contained two compartments that could be isolated from one another by varying the total volume of solution in the chamber. One compartment was used for placing the coverslip with cells, whereas the other one was used for placing the theta tube and the patch pipette during recordings. The latter compartment was continuously perfused using a gravity-fed system, whereas the solutions flowing through the theta tube were pressure driven (ALA BPS-8; ALA Scientific Instruments). To estimate the time course of the solution exchange, the change in liquid junction potential was periodically measured with an open-tip patch pipette (Fig. 4). During experiments, the same KCl-based solution was used in the patch pipette, in both barrels of the theta tube, and in the gravity-fed perfusion; its composition was (in mM) 142 KCl, 5.4 NaCl, 1.8 $CaCl_2$, 1.7 mM $MgCl_2$, 10 mM HEPES/KOH, pH 7.4. In addition, during macroscopic current recordings, the solution flowing through one of the theta tube barrels also contained 100 μM ACh. During (steady-state) single-channel recordings, both in the cell-attached and outside-out configurations, the solution bathing the extracellular aspect of the patch also contained 30–100 nM ACh. Both macroscopic and single-channel currents were recorded with an Axopatch 200B amplifier (Molecular Devices) at −80 mV and room temperature (∼22°C), and were digitized at 100 kHz. Series resistance compensation was used and set to 70–80% during all macroscopic recordings. The effective bandwidth before data analysis was DC-10 kHz for macroscopic currents, and DC-20 kHz for single-channel currents.

Data Analysis

Macroscopic currents were analyzed using a combination of pClamp 9.0 (Molecular Devices), SigmaPlot 7.101 (SPSS Inc.), and in-house developed programs, whereas single-channel currents were analyzed using the SKM-MIL combination in QuB software (Qin and Auerbach, 1996; Qin, 2004; www.qub.buffalo.edu).

The expressions describing the time courses of the different states in Fig. 1 were obtained by numerically computing the eigenvalues and eigenvectors of the corresponding Q-matrix (using Maple 6 software, Maple Waterloo, Inc.), following the methods described by Colquhoun and Hawkes (1995). On the other hand, the expressions describing the time courses of the different states in the simplified scheme in Fig. 9 A (used for Fig. 6, Fig. 9 B, and Fig. 10, A–D) were obtained by analytically solving the corresponding set of differential equations.

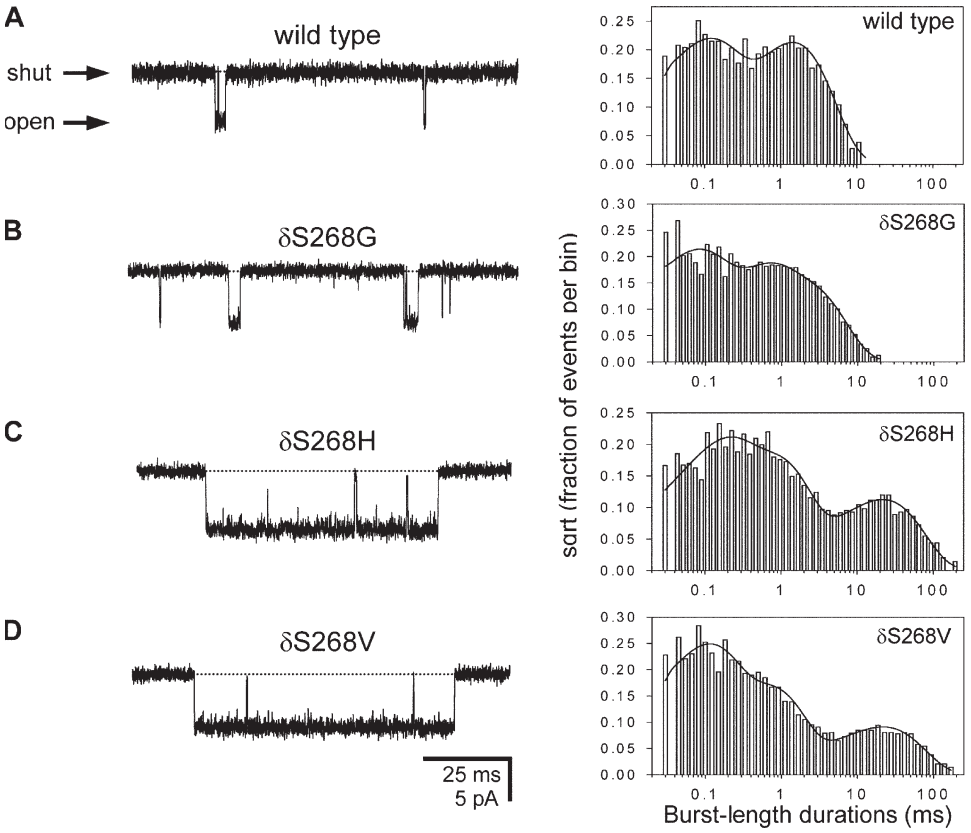

Figure 3. Burst length distributions. Example bursts of single-channel openings, and burst length duration histograms corresponding to recordings obtained from individual patches. Currents were recorded at −80 mV in the steady presence of 100 nM ACh. Openings are downward deflections. Display $f_c \cong 6$ kHz. The zero-current level is indicated, on each trace, with a dotted line. Bursts were defined using the criterion of Jackson et al. (1983) as outlined in Materials and methods. The time constant of the slowest component of the burst length distribution, the t_{crit} value, the total number of analyzed events (i.e., openings plus shuttings), and the fraction of misclassified shuttings in the particular cases shown are, respectively: (A) 1.29 ms, 0.27 ms, 5,691, 0.0022; (B) 1.76 ms, 0.22 ms, 25,505, 0.054; (C) 19.5 ms, 1.48 ms, 11,493, 0.047; (D) 19.6 ms, 0.85 ms, 10,183, 0.028. The plotted bursts, especially in the cases of the His and Val mutants, are among the longest bursts in their respective distributions. The "length" of a burst includes the durations of all openings and shuttings within it.

The slowest time constant values of single-channel closed≡open burst-length distributions (Fig. 2 B) were computed from the estimates of transition rates with approximate allowance for missed events (Qin et al., 1996). In turn, these transition rates were estimated by fitting the rate constants of uncoupled-type kinetic models (Rothberg and Magleby, 1998) to the idealized sequences of dwell times using full maximum-likelihood methods (Qin et al., 1996). Bursts were defined as series of (one or more) openings separated by shuttings shorter than a critical time (t_{crit}). A separate t_{crit} value was determined for each patch, on the basis of the corresponding shut-time distribution, using the criterion proposed by Jackson et al. (1983) with only minor modifications (Purohit and Grosman, 2006). Particularly in the case of the gain-of-function mutants, not only brief (a few tens of microseconds), but also longer (hundreds of microseconds) shuttings appeared to separate openings within a burst. These longer shuttings, which are too long to be ascribed to sojourns in the closed diliganded state, have been consistently observed in recordings from gain-of-function AChR mutants (Grosman and Auerbach, 2001). Although their origin is unclear, these shuttings were considered to be part of a burst when calculating t_{crit} values.

The kinetics of entry into desensitization of the different constructs are expressed in terms of desensitization half-times (Table I). These, in turn, were calculated from the parameters of mono- or double-exponential fits to the decaying phase of the macroscopic current response to step changes in the ACh concentration from 0 to 100 μM (Fig. 7 and Fig. 11 B). The use of these phenomenological "half-times" was necessary, here, because we needed to somehow compare the time courses of desensitization of the analyzed constructs. And although the wild-type AChR and some of the mutants desensitize following a monoexponential time course, others do so with double-exponential kinetics. Of course, when a time course is best described by a double-exponential function, nothing exact can be done to compare it with the kinetics of a monoexponential time course. We found, however, that the half-decay times ($t_{1/2}/ln2$, more precisely), obtained from the parameters of the double-exponential fits, provide an excellent approximation to the desensitization time course during the first tens of milliseconds. In other words, when we plot the experimentally obtained double-exponential desensitization decays and the monoexponential decays calculated from the respective $t_{1/2}$ values, we find a very close agreement between both curves during the first tens of milliseconds. After these initial milliseconds, the time courses deviate from one another, but it is these initial tens of milliseconds that matter in the context of the 50-Hz trains (i.e., 20-ms interpulse intervals) applied here. Hence, mono- and double-exponential desensitization time courses are compared using their corresponding half-times.

RESULTS

Gain-of-Function Mutants of the Muscle AChR Desensitize during Channel Deactivation

Although previous single-channel data recorded from a series of gain-of-function AChRs were consistent with the existence of pathways other than just ACh dissociation from the closed state for the termination of endplate

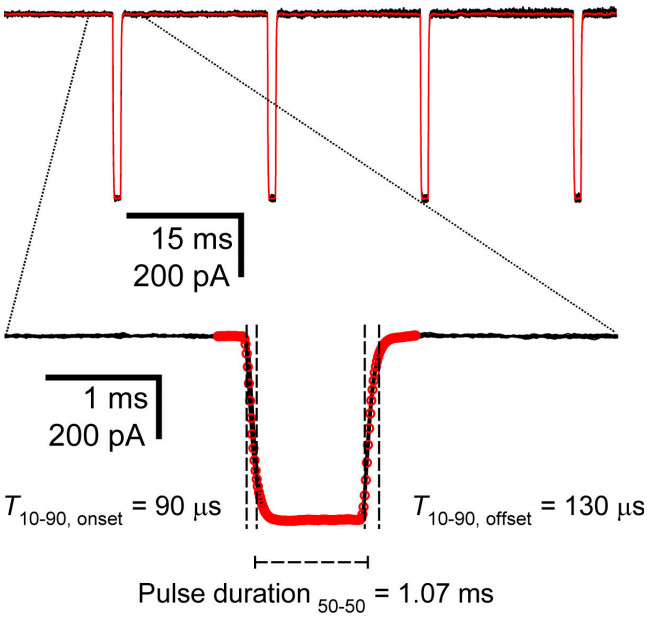

Figure 4. Calibration of the solution-switching system. The different parameters of the solution-switching system (i.e., diameter of the theta tube openings, relative positioning of the theta tube and patch pipette, flow rate of solutions, bandwidth of the computer-generated waveform) were adjusted so as to optimize the time course of the solution exchange. The latter was estimated by measuring the liquid junction potential by alternatively exposing the tip of an open pipette to 1 M KCl (for ~1 ms) and 140 mM KCl (for ~20 ms) solutions. In this particular recording, 48 1-M pulses were applied. The trace was segmented in 12 groups of four pulses, and these were aligned and averaged (red trace). The 10–90% risetime during both the onset and the offset, as well as the duration of exposure to the 1 M KCl solution, are indicated for this representative recording.

currents (Grosman and Auerbach, 2001), the specific suggestion that desensitization contributes to deactivation was based on rather indirect observations (i.e., kinetic analysis of single-channel currents). To define this issue in an unequivocal manner, we applied trains of brief (1 ms) ACh pulses (100 µM) at different frequencies to outside-out patches expressing wild-type or gain-of-function AChRs. In these experiments, receptor desensitization is expected to be manifest as a frequency-dependent decrease in the peak value of succesive macroscopic current responses, as the availability of activatable receptors diminishes along the train.

Fig. 5 shows example traces recorded from eight gain-of-function adult-type mutants (Thr, Cys, Glu, Asp, His, Val, Asn, or Gln substituting for the wild-type Ser at position 12' of the δ-subunit M2 segment) exposed to 1-s, 50-Hz trains. These mutations affect mostly the kinetics of gating, speeding up channel opening and slowing down channel closure (i.e., the mutations increase β_2 and decrease α_2; Fig. 1; Grosman and Auerbach, 2000, 2001). Traces recorded from the adult wild-type AChR (i.e., containing the ε subunit), as well as from its fetal counterpart (containing the γ subunit, instead of ε), and the Ala and Gly

TABLE I

Kinetic Parameters of a Gain-of-Function Mutant Series

Construct	$\tau_{deactivation}$ [a]	$\tau_{slowest}$ [b]	$t_{1/2,\ desensitization}$ [c]	Paired-pulse $\tau_{recovery}$ [d]	Train $\tau_{recovery}$ [e]
	ms	ms	ms	ms	ms
δS268A	0.72 ± 0.02 (7)	0.95 ± 0.08 (2)	34 ± 8 (4)	ND	1,333 (3)
wild-type/ε	0.99 ± 0.08 (13)	1.20 ± 0.06 (3)	26 ± 4 (8)	306 ± 19 (5)	500 (6)
δS268G	1.4 ± 0.1 (10)	1.85 ± 0.09 (2)	11 ± 4 (4)	ND	286 (4)
wild-type/γ	4.6 ± 0.5 (10)	5.7 ± 0.5 (4)	31 ± 12 (3)	290 ± 33 (4)	167 (4)
δS268T	7.5 ± 0.8 (7)	11.6 ± 1.5 (2)	91 ± 19 (4)	ND	182 (5)
δS268C	8.0 ± 0.1 (7)	10.33 ± 0.09 (2)	72 ± 6 (6)	478 ± 25 (4)	444 (4)
δS268E	12.4 ± 0.5 (2)	13.2 ± 0.2 (2)	45 ± 10 (4)	ND	500 (4)
δS268D	15.4 ± 0.1 (2)	26 ± 2 (9)	92 ± 25 (4)	ND	1,000 (3)
δS268H	16 ± 2 (2)	23 ± 3 (2)	30 ± 6 (4)	ND	364 (3)
δS268V	18.7 ± 0.3 (12)	20.1 ± 0.6 (2)	104 ± 19 (2)	316 ± 16 (4)	400 (2)
δS268N	24 ± 2 (18)	44 ± 4 (11)	70 ± 13 (5)	497 ± 25 (6)	500 (7)
δS268Q	28 ± 1 (2)	36 ± 2 (11)	42.1 ± 0.1 (2)	ND	333 (2)

ND, not determined.

[a]Deactivation time constants estimated from monoexponential fits. The numbers in parentheses indicate the number of <1-Hz trains of 1-ms, 100 µM ACh pulses analyzed. Each train consisted of at least 10 such pulses, the responses to which were averaged and fitted. Average values across trains are given as mean ± standard error.

[b]Time constants of the slowest component of single-channel burst length distributions. The numbers in parentheses indicate the number of patches (both cell-attached and outside-out) analyzed.

[c]Desensitization half-times. In some cases, the time course of entry into desensitization was best fitted with two (rather than one) exponential components. Hence, for easier comparison, the parameters of these fits (whether single or double exponential) were used to numerically solve for the corresponding desensitization half-times (i.e., the time taken for the current decay to be half complete). The numbers in parentheses indicate the number of responses averaged.

[d]Recovery-from-desensitization time constants estimated from the response to paired-pulse protocols. The numbers in parentheses indicate the number of patches analyzed to generate the plots in Fig. 8 B.

[e]Recovery-from-desensitization time constants estimated from the fitting of the mechanism in Fig. 9 A directly to plots of normalized peak current vs. pulse number (Fig. 6). The numbers in parentheses indicate the number of responses analyzed to generate these plots.

substitutions at δ-M2 12' (both with little effect on gating), are also shown in this figure. The plots are arranged, from δS268A to δS268Q, in increasing order of deactivation time constant (Table I). Fig. 6 shows the average response of patches expressing each of these constructs.

Together, these results lend support to the hypothesis that gain-of-function mutations increase the probability of the AChR entering a desensitized conformation

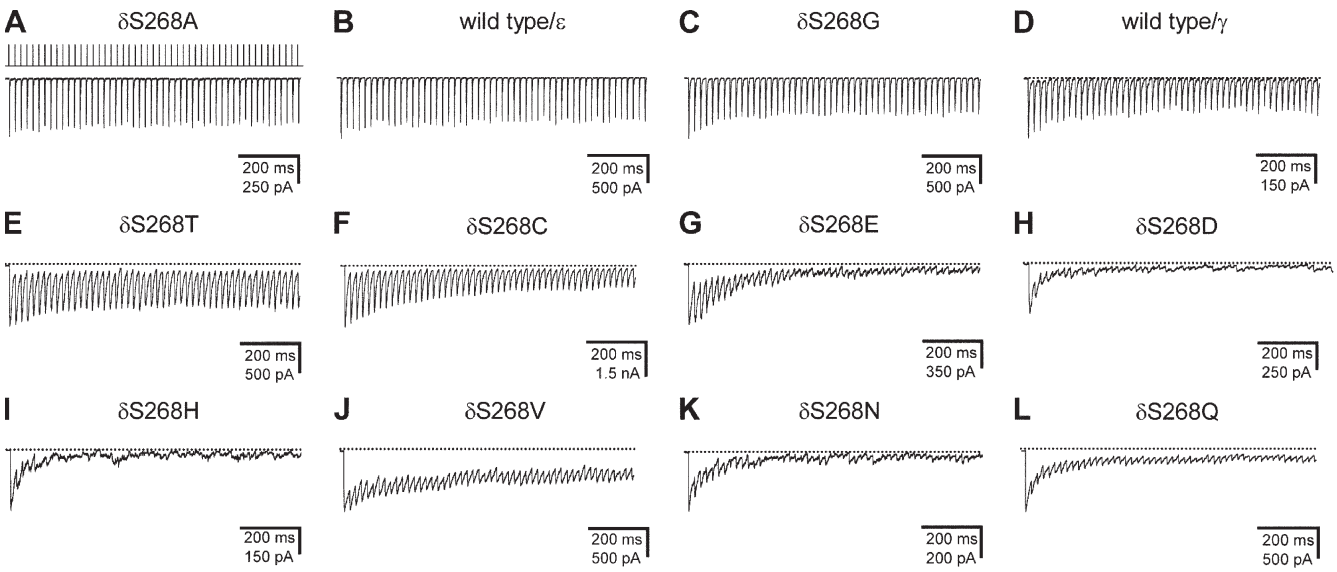

Figure 5. Gain-of-function AChR mutants desensitize during deactivation. The hypothesis that mutant AChRs desensitize upon neurotransmitter removal was tested in the outside-out configuration with the application of high-frequency trains of brief ACh pulses. (A–L) Example current traces from individual patches. Each panel is the response of a different construct to the application of a 50-Hz train of 1-ms, 100 μM ACh pulses. One such trains is indicated in A above the current trace. The zero-current level is indicated, on each trace, with a dotted line. The plots are presented in increasing order of deactivation time constant (Table I). The prediction of Eq. 2, namely that (everything else being equal) the slower the deactivation time course, the more pronounced the depression, is borne out by these recordings. Of course, because the kinetics of entry into and recovery from desensitization are not completely unaffected by the mutations (i.e., "everything else" is not exactly equal; Table I), this relationship cannot be perfect. However, the trend is, undoubtedly, clear (see also Fig. 6).

during deactivation (Eq. 2). It is clear that kinetic mechanisms that ignore desensitization as a pathway for closed≡open burst termination cannot explain these findings. Moreover, the results in Figs. 5 and 6 are consistent with the assumption (Eqs. 1 and 2) that desensitization of the diliganded wild-type AChR can only proceed from the open state. Evidently, if desensitization proceeded only from the closed state (as suggested for other neurotransmitter-gated ion channels), the extent of desensitization upon neurotransmitter removal would not increase as the β_2/α_2 ratio (see Fig. 1) does (i.e., in going from δS268A to δS268Q).

It could be argued that the behavior illustrated in Figs. 5 and 6 can also be due to other factors, in addition to the increase in the β_2/α_2 ratio upon mutation (Eq. 2). Certainly, a faster rate constant of entry into desensitization and/or slower kinetics of recovery from desensitization upon ACh removal ($DA_2 \rightarrow DA \rightarrow D \rightarrow C$ or $DA_2 \rightarrow DA \rightarrow CA \rightarrow C$; Fig. 1) would contribute to the progressive depression of the macroscopic peak currents observed. And, although large changes in the kinetics of entry into desensitization were not evident in previous cell-attached single-channel recordings from these mutants (Grosman and Auerbach, 2001), the kinetics of recovery upon neurotransmitter washout cannot be studied during steady applications of neurotransmitter.

To study the effect of the tested mutations on the kinetics of entry into desensitization, we exposed outside-out patches to step changes in the concentration of ACh from 0 to 100 μM (Fig. 7), and analyzed the decaying phase of the resulting current transients (Table I). The time constant(s) governing this current decay reflects the rate constant(s) of entry into desensitization without much interference from the kinetics of gating, reopening of desensitized receptors, or ACh binding and unbinding. This is because (a) the diliganded gating equilibrium constant values of the wild-type and mutant AChRs studied here are large (>15), (b) reopening of diliganded desensitized receptors is comparatively slow, (c) desensitization of diliganded AChRs proceeds mainly from the open state, and (d) a value of 100 μM for the concentration of ACh is high enough to temporally segregate the time course of ACh binding (which occurs, largely, during the rising phase of the transient) from that of desensitization (which occurs, largely, during the decaying phase). We can illustrate this point with a simple calculation. For example, using the full model of Fig. 1 and adult wild-type values (which include a value of $\sim 25\ s^{-1}$ for the $OA_2 \rightarrow DA_2$ rate constant and zero values for the other five rate constants of entry into desensitization), it can be calculated (using Q-matrix methods; Colquhoun and Hawkes, 1995) that upon stepping the concentration of ACh from 0 to 100 μM, the decaying phase of the current transient would be dominated by an ∼46-ms time constant. Indeed, the value of this time constant is quite close to 40 ms, that is, the reciprocal of the $OA_2 \rightarrow DA_2$ entry-into-desensitization rate constant. Of course, the use of ACh concentrations

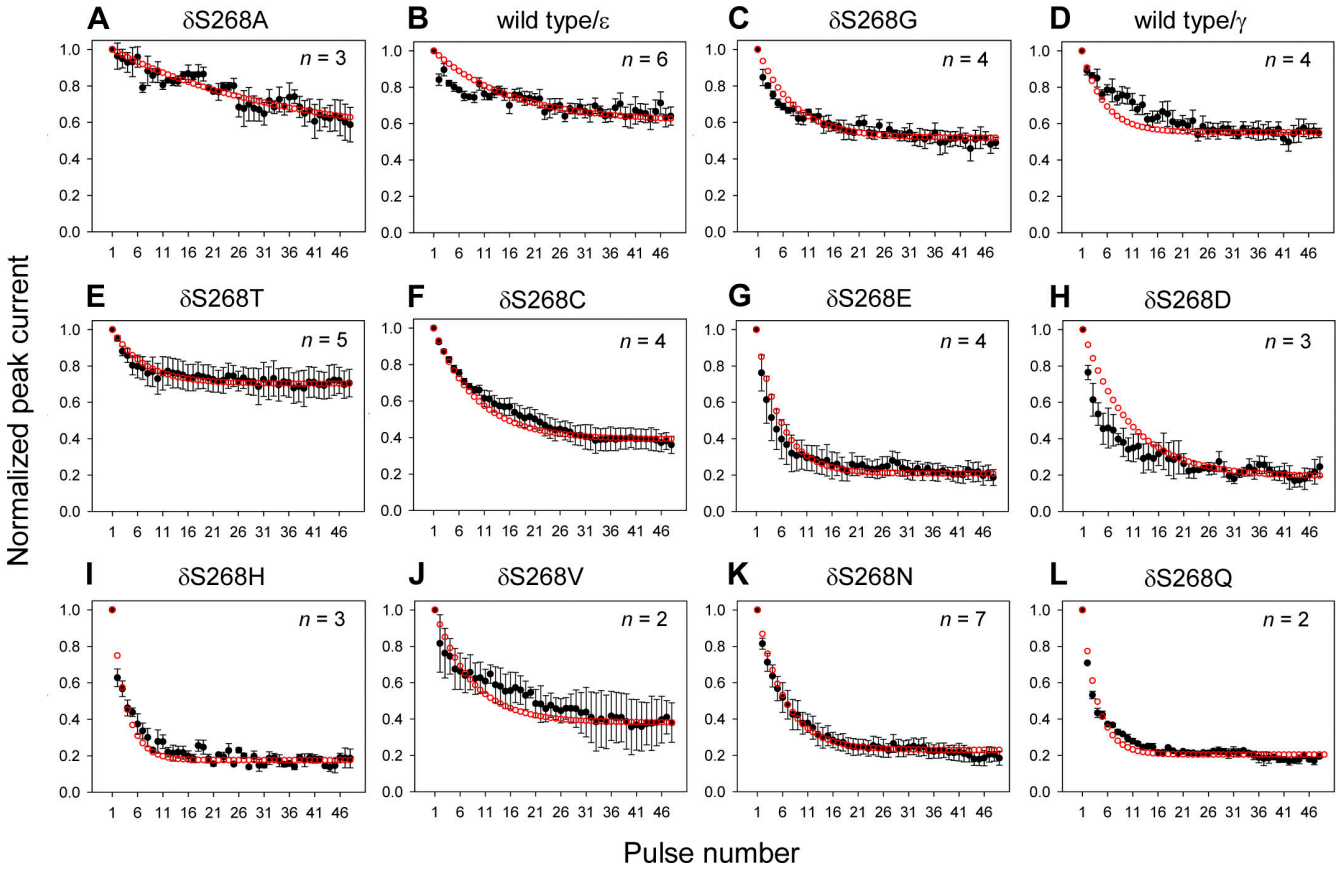

Figure 6. Depression of ACh-evoked currents upon repetitive stimulation. (A–L) Peak current values in response to 50-Hz trains of 1-ms, 100 μM ACh pulses were normalized with respect to the first peak in each series and averaged (black circles). The number of averaged responses (n) is indicated. Vertical error bars are standard errors. Example current traces for each construct are given in Fig. 5. The red circles correspond to the fits with the reaction scheme in Fig. 9 A (see Results). For each construct, the fitted parameter was the value of the recovery rate constant (Desensitized→Activatable; expressed as their reciprocals in Table I). The values of the other variables needed for these fits were taken from the experimental data, as follows. The sum of the rate constants leading away from the activated states was calculated as the reciprocal of the deactivation time constant of each construct (Table I). The value of the (single) entry-into-desensitization rate constant (note that desensitization of activated receptors occurs as a single-step isomerization in this scheme) was calculated from the half-time values in Table I, as $(ln2)/t_{1/2}$. In turn, these half-times were calculated as explained in Materials and methods and in the legend to Table I. For those mutants displaying double-exponential desensitization time courses, the use of a single desensitization rate constant is, of course, an oversimplification. However, it can be shown that the monoexponential decays calculated using these half-times approximate very well the experimentally obtained double-exponential desensitization time courses during the first tens of milliseconds (see Materials and methods).

>100 μM would be more effective at temporally separating ACh binding from desensitization (and would, thus, allow more accurate estimates of the entry-into-desensitization rate constant) but pore blockade ($K_{B,\,ACh} \cong 2.0$ mM at −80 mV) would, then, become a new problem. Therefore, sustained applications of 100 μM ACh seem appropriate to probe the effect of mutations, specifically, on the entry-into-desensitization rate constant of open, diliganded AChRs. The experimentally obtained values in Table I (expressed as desensitization half-times, as explained in Materials and methods) clearly show that, if anything, entry into desensitization is slower in these gain-of-function mutants, not faster.

The effect of the mutations on the kinetics of recovery, on the other hand, was assessed using pairs of conditioning (1 s) and test (100 ms) 100 μM ACh pulses separated by intervals of variable duration (Fig. 8 and Table I). The long duration and high ACh concentration during the conditioning pulse ensured that the macroscopic currents decayed almost completely before the ACh washout interval started. In this manner, entry into and recovery from desensitization are dissected, the former occurring during the conditioning pulse, and the latter occurring during the interval between the conditioning and test pulses. The important caveat here, though, is that the kinetics of recovery are known to depend on the duration of the conditioning pulse (Reitstetter et al., 1999; Elenes and Auerbach, 2002) and, thus, our particular paired-pulse protocol, using 1-s conditioning pulses, may not really have probed the kinetics of recovery that are relevant during a high-frequency train of brief ACh pulses. During such trains,

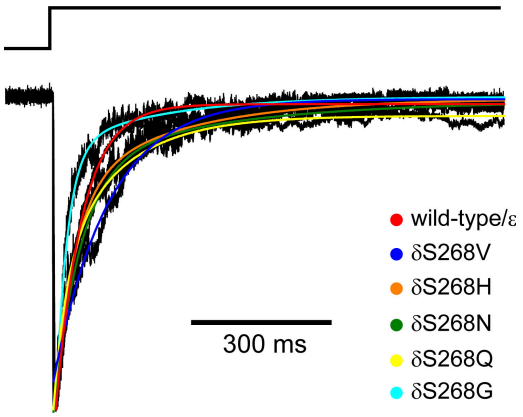

Figure 7. AChR desensitization. The kinetics of entry into desensitization were estimated by exposing outside-out patches (−80 mV) to 2-s, 100 μM ACh pulses. As shown by the example current traces, opening is a transient event. For clarity, only the responses of some of the studied constructs are shown. All traces were aligned and normalized, and their decaying phases were fitted (least-squares method) from the peak of the currents until the end of the 2-s ACh applications with one or two exponential components (only the first second is shown). The parameters of these fits were used to calculate desensitization half-times (see Materials and methods). The corresponding averages, over a number of responses per construct, are listed in Table I.

the neat separation between entry into desensitization and recovery is lost because both phenomena occur during the interpulse intervals, when the concentration of ACh is close to zero. The problem of estimating the kinetics of recovery within a train of neurotransmitter pulses is addressed in the sections below.

A Quantitative Description of the Response of the Muscle AChR to Trains of ACh Pulses

To gain a clearer insight into what happens during the deactivation phase of macroscopic currents upon repetitive exposure to ACh, we analyzed the kinetic scheme in Fig. 9 A, a simplified version of that in Fig. 1. In this reduced scheme, the various states in Fig. 1 are grouped into activated (CA_2 and OA_2), activatable (C and CA), and desensitized (D, DA, and DA_2) sets of states. Furthermore, since unliganded and monoliganded open channels (O and OA) close very fast, they are considered to be part of the activatable pool of receptors, as well. One of the main advantages of using this simplified model is that the time courses of the three relevant sets of states upon stepping the ACh concentration to zero (i.e., activated, activatable, and desensitized) can be expressed as rather simple analytical expressions.

We can assume that, in the absence of ACh, all AChRs are closed and, therefore, activatable. Thus, upon stepping the ACh concentration from zero to a high-concentration value, most receptors become rapidly diliganded (i.e., activated), as they quickly bind the applied ACh. On termination of the pulse, activated channels keep oscillating between the diliganded closed and open conformations until they either lose the bound ACh (Activated→Activatable) or adopt a desensitized conformation (Activated→Desensitized). Desensitized receptors, in turn, can recover while the concentration of ACh remains at near-zero levels, thus joining the pool of activatable receptors (Desensitized→Activatable). Fig. 9 B shows the calculated time course of interconversion among the activated, activatable, and desensitized sets of states during one example interpulse interval for a hypothetical gain-of-function AChR. On arrival of the following pulse of ACh, activated receptors remain activated, desensitized receptors stay desensitized and become fully liganded, and most activatable receptors become activated, as they bind the newly applied ACh.

Fig. 10 (A–D) shows the predicted effect of the different variables (i.e., deactivation time constant, rate

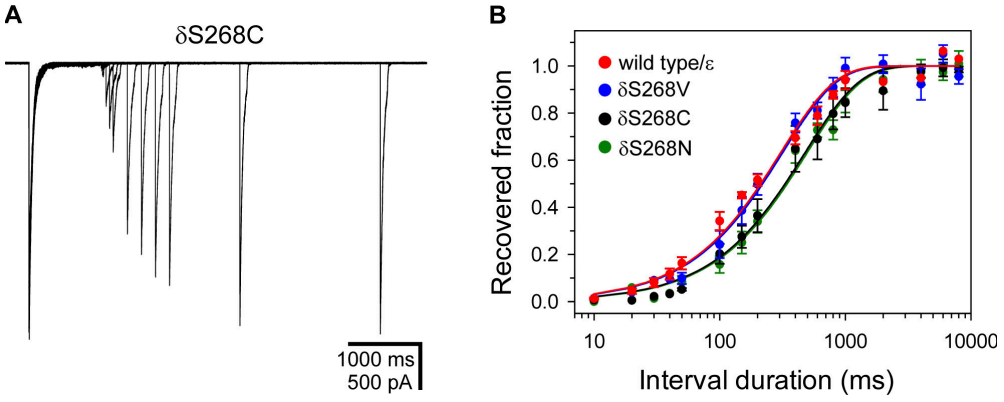

Figure 8. AChR recovery from desensitization. The kinetics of recovery from desensitization were estimated using pairs of conditioning and test, 100 μM ACh pulses (1 s and 100 ms in duration, respectively) with intervening intervals of variable length. Desensitization was nearly complete at the end of each conditioning pulse; hence, recovered-fraction values were estimated as the ratio between the peak current elicited by the test pulse and that elicited by the conditioning pulse in each pair. The interval between any two consecutive pairs of pulses was ≥6 s to ensure complete recovery from desensitization. (A) A representative recording from the δS268C mutant. (B) Plots of recovered fraction as a function of the duration of the interpulse interval were well fitted with monoexponential rise functions in spite of the multiple steps that must be involved in the recovery of ACh-diliganded desensitized receptors (i.e., DA_2→DA→D→C or DA_2→DA→CA→C); the corresponding time constants are listed in Table I. Vertical error bars are standard errors. The kinetics of recovery within trains of pulses were estimated as indicated in Fig. 6.

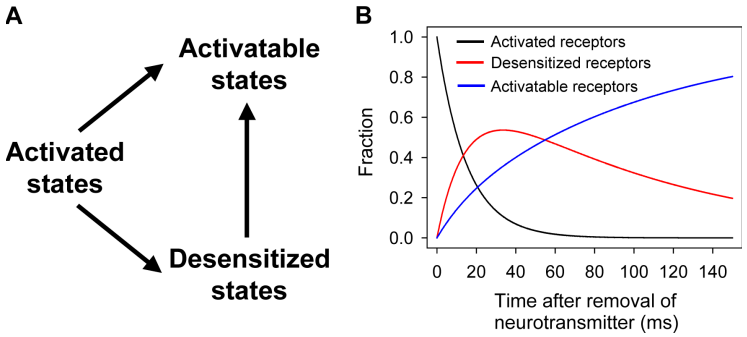

Figure 9. A mechanistic view of AChR deactivation. (A) A simplified version of the reaction scheme in Fig. 1. This scheme was used to interpret the response of the AChR during zero-ACh, interpulse intervals. The correspondence between states in Fig. 1 and sets of states in this reduced model is explained in Results. Upon ACh removal, receptors in activated states either lose ACh (becoming activatable) or desensitize. Desensitized receptors, in turn, can recover and become activatable. All three steps in this kinetic scheme can be considered to be unidirectional because, in the absence of ACh (a) ACh rebinding cannot occur, (b) diliganded desensitized receptors are much morelikely to recover than to reopen, and (c) activatable receptors do not desensitize much; hence, the single arrows. In this model, the deactivation time constant is the reciprocal of the sum of the two rate constants leading away from the activated states. Consistent with the experimental observations, this model predicts monoexponential time courses of deactivation and recovery from desensitization. Also, consistent with the behavior of wild-type AChRs and of some of the mutants, the predicted time course of entry into desensitization is monoexponential, as well. (B) Kinetics of interconversion among the different sets of states in A upon stepping the concentration of ACh to zero. The time course of each set of states in this "triangular" kinetic scheme was solved analytically (see Materials and methods), and is plotted for a hypothetical gain-of-function mutant (deactivation time constant = 15 ms; entry-into-desensitization rate constant = 50 s^{-1}; recovery rate constant = 10 s^{-1}). The concentration of ACh is stepped to 0 at time zero. All receptors are assumed to be activated before this concentration jump.

constants of entry into and recovery from desensitization, and stimulation frequency) on the response of a hypothetical ensemble of channels to a train of neurotransmitter pulses. It can be seen that, at a given train frequency, a slower deactivation (Fig. 10 A), a faster entry into desensitization (Fig. 10 B), and a slower recovery (Fig. 10 C) all lead to a more profound depression of the macroscopic current response.

A salient feature of the response of multichannel outside-out patches to high-frequency repetitive stimulation is that the decline in the peak current values continues until a nonzero plateau level is attained (Figs. 5 and 6). This is compelling evidence that desensitized receptors recover appreciably during the 20-ms interpulse intervals. Indeed, if this recovery were negligible, then this decline would continue until no more currents can be elicited by subsequent pulses. Early in each train, the peak current values decrease because the number of receptors that desensitize exceeds the number of receptors that recover. However, the number of receptors that desensitize during interpulse intervals decreases, whereas the number of receptors that recover increases, along a train. Eventually, these two numbers become equal, and the peak current reaches a steady-state value. Fig. 10 (E and F) shows experimental data (of the kind shown in Fig. 6) recorded at different train frequencies from two of the gain-of-function mutants. Reassuringly, the observed depression of peak currents displays the frequency dependence predicted by Fig. 10 D. That is, as the frequency of the stimulation train increases, the steady-state peak current level decreases, eventually becoming equal to the steady-state current in response to a sustained application of neurotransmitter.

As mentioned above, when the response within a stimulation train is under study, the recovery that matters is the one occurring during the interpulse intervals. To estimate its kinetics in the different constructs, we "fitted" the experimental observations in Fig. 6 with the simplified mechanism in Fig. 9 A. We did this, essentially, as for Fig. 10, calculating the fraction of channels that become activated upon each consecutive pulse, using the analytical expressions for the time courses of the different sets of states. In this particular case, though, the rate/time constants of deactivation and entry into desensitization of each construct were taken from their experimentally estimated values (Table I), the interpulse interval was fixed at 20 ms, and the (unknown) value of the recovery rate constant (i.e., the rate constant governing the Desensitized→Activatable step in Fig. 9 A) was varied manually until a reasonably good fit (judged by eye) to the experimental data in Fig. 6 (black circles) was reached. The fits are shown with red circles in Fig. 6, and the estimated recovery rate constants are listed in Table I, expressed as their reciprocals (for easier comparison with the time constant estimates obtained from paired-pulse protocols). Somewhat unexpectedly, we found that the kinetics of recovery during interpulse intervals are not very different from those after 1-s exposures to 100 μM ACh. Perhaps, even longer applications of ACh (>1 s) are needed for the AChR to adopt the more reluctant, slower-to-recover conformations reported in the literature (Reitstetter et al., 1999).

A cursory inspection of Table I indicates that the tested mutations affect mostly the kinetics of deactivation; the kinetics of entry into and recovery from desensitization are affected to a much smaller degree. We conclude, then, that it is mainly the higher β_2/α_2 ratio of these mutants that underlies the larger extent of desensitization (Eq. 2). In other words, the comparatively small depression of the macroscopic currents observed upon repetitive stimulation of the wild-type AChR is due, not to desensitization being exceedingly slow or to

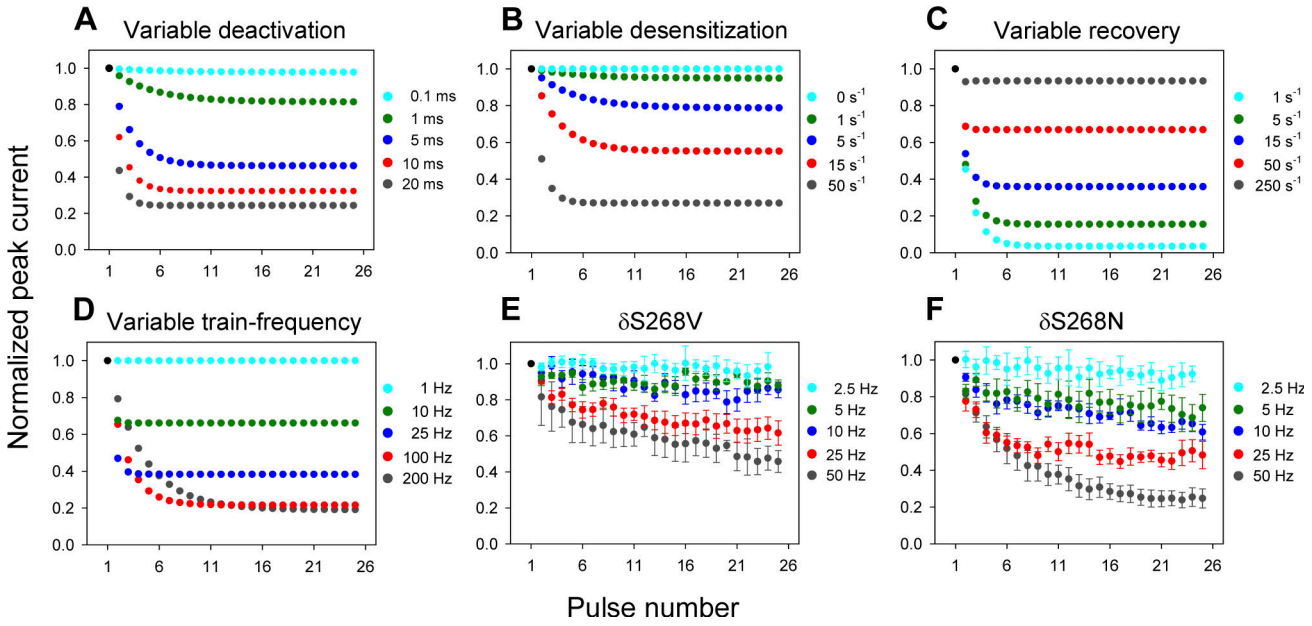

Figure 10. Effect of different variables on the macroscopic response to trains of brief neurotransmitter pulses. (A–D) Normalized peak current values under different hypothetical situations. These plots were generated by analytically solving for the fraction of channels that become activated upon each successive pulse, using the kinetic scheme in Fig. 9 A. Although these calculations do not distinguish between activated closed (CA_2) and activated open (OA_2) receptors, the fraction of activated channels that are open is expected to be large in the case of wild-type and gain-of-function mutant AChRs (~0.95 in the case of the adult wild-type receptor). Thus, the calculated fraction of activated channels is a good approximation to the fraction of open channels. Unless otherwise indicated, $\tau_{deactivation}$ = 15 ms, desensitization rate constant = 50 s^{-1}, recovery rate constant = 10 s^{-1}, and train frequency = 50 Hz. Each arriving pulse of ACh is considered to be too short for desensitization within a pulse to be appreciable, and is assumed to convert all activatable receptors into activated ones. The latter is a very good approximation because, using the full model in Fig. 1 and adult wild-type rate constant values, it can be calculated (using Q-matrix methods; Colquhoun and Hawkes, 1995) that ~90% of all activatable AChRs would be activated by the end of a 1-ms, 100 μM ACh pulse. (E and F) Experimental data from two of the gain-of-function mutants exposed to trains of different frequencies. Vertical error bars are standard errors. The y axis value corresponding to the first pulse in each train (black circles) is the same for all trains.

recovery being extremely fast but, rather, to its gating equilibrium constant not being large enough.

Naturally-Occurring Gain-of-Function Mutants also Desensitize during Channel Deactivation

Gain-of-function mutations to the AChR occur naturally. These mutations often lead to a neuromuscular disorder known as slow-channel congenital myasthenic syndrome, characterized by weakness and fatigability of voluntary muscles (Engel et al., 2003). In light of our results with lab-engineered mutations, it seemed sensible to wonder whether desensitization contributes to the deactivation time course of these naturally occurring mutants as well. The results in Fig. 11 amply confirm this prediction, at least for the εT264P mutation (Ohno et al., 1995; position ε264 is the 12' position of εM2). Despite this mutant's much slower kinetics of entry into desensitization ($t_{1/2,\,desensitization} \cong [106 \pm 17]$ ms; Fig. 11 B), closely timed applications of ACh elicit increasingly smaller macroscopic currents (Fig. 11 D). Once again, this is fully consistent with the prolonged deactivation time course of this mutant ($\tau_{deactivation} \cong [28 \pm 2]$ ms; Fig. 11 A).

DISCUSSION

The main finding of this paper is that gain-of-function mutations increase the extent to which AChRs desensitize during deactivation. This is important because most of the mutations that have been engineered, thus far, to probe the relationship between structure and function of the muscle AChR lead to gain-of-function phenotypes, and the functional impact of these mutations is (in the best cases) inferred from steady-state kinetic modeling studies in which desensitization is usually ignored. One clear concept that emerges from this study is that, although this useful simplification is certainly valid in the wild type, the extent to which a diliganded closed≡open burst is curtailed by entry into desensitization is considerable in mutants of the gain-of-function type (Figs. 5 and 6). In other words, if it were not for desensitization, endplate currents through gain-of-function mutants would decay even more slowly. For example, in the case of the Gln mutant (δS268Q), it can be calculated (using Eq. 1 and the values in Table I) that, if desensitization did not contribute to channel deactivation, the deactivation time constant would be ~52 ms,

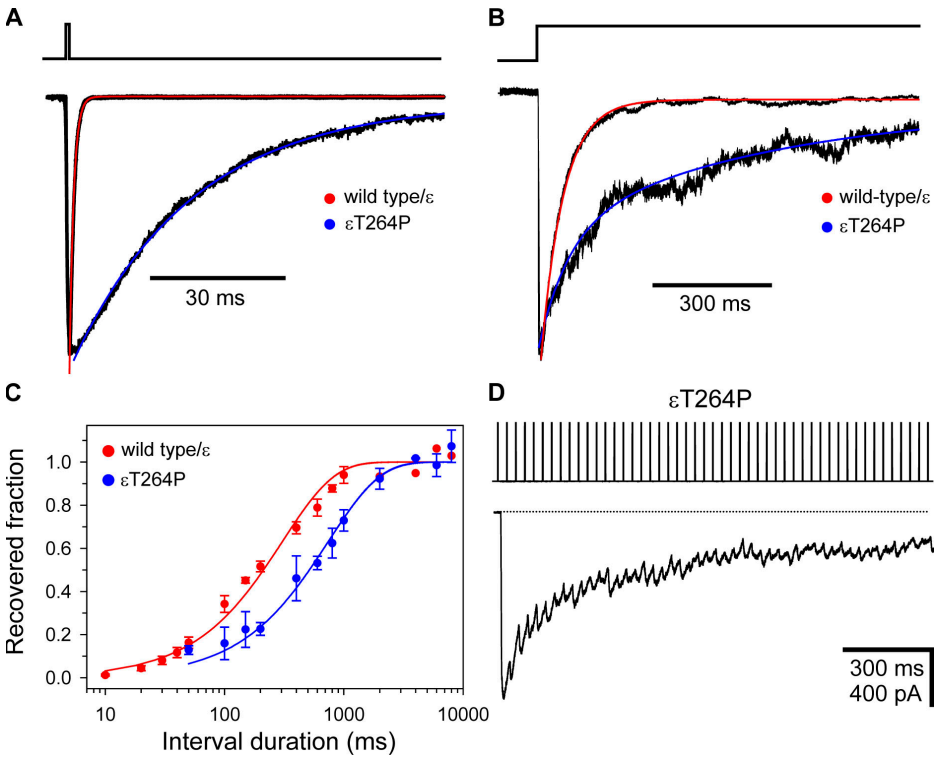

Figure 11. A naturally occurring gain-of-function mutant desensitizes during deactivation. (A) The kinetics of deactivation were estimated and analyzed as described in Fig. 2 A. The plotted trace is the average response of a patch expressing the εT264P mutant to 10 1-ms, 100 μM ACh pulses applied as a 0.33-Hz train. The response of the adult wild-type AChR is also shown for comparison. The deactivation time constant of this mutant, averaged over a number of such trains, is 28 ± 2 ms (mean ± SEM, n = 5 trains), whereas that of the adult wild-type receptor is 0.99 ± 0.08 ms (mean ± SEM, n = 13 trains). (B) The kinetics of desensitization were estimated and analyzed as described in Fig. 7. The response of the adult wild-type AChR is also shown for comparison. In five out of six patches expressing this mutant, the best fit to the decaying phase was obtained with two exponential components. The desensitization half-time of the mutant, averaged over these six patches, is 106 ± 17 ms (mean ± SEM), whereas that of the adult wild-type receptor is 26 ± 4 ms (mean ± SEM, n = 8 patches). (C) The kinetics of recovery from desensitization were estimated and analyzed as described in Fig. 8. Vertical error bars are standard errors. The recovery time constant of the mutant is 742 ± 37 ms (data points from two patches), whereas that of the adult wild-type receptor is 306 ± 19 ms (data points from five patches). (D) Example current trace in response to a 50-Hz train of 1-ms, 100 μM ACh pulses. The zero-current level is indicated with a dotted line.

almost twice as long as the measured value. Thus, the effect of desensitization on the observed channel kinetics should not be disregarded. Evidently, physically realistic conclusions (i.e., the only kind of conclusion that can help us understand how structure gives rise to function) can only be drawn in the framework of correct kinetic mechanisms. More generally, our results underscore the critical importance of complementing the insight provided by steady-state applications of agonist with that stemming from concentration-jump experiments.

Another reason why the finding we report here is important is that desensitization can limit the availability of activatable receptors during repetitive stimulation. Indeed, it is quite tempting to extrapolate our results to a more physiological situation and entertain the possibility that gain-of-function AChRs accumulate in desensitized conformations also in the context of an intact neuromuscular junction, in response to high-frequency action potential firing. Further, it is intriguing to ponder that this depression might contribute to the impaired neuromuscular transmission that characterizes the slow-channel congenital myasthenic syndrome.

However, it is important to realize here that, unlike the situation in the outside-out patch-clamp configuration, the quanta of neurotransmitter released by a presynaptic neuron do not impinge on exactly the same subset of postsynaptic receptors every time an action potential arrives. Therefore, any given receptor interacts with the neurotransmitter at only a fraction of the firing frequency and, eventually, only once per burst of action potentials. This is relevant because, as shown by the outside-out recordings in Fig. 10 (E and F), the extent of depression decreases as the frequency of stimulation is reduced. The question, then, arises as to how much lower this "effective frequency" gets to be.

The value of this effective frequency depends directly on the degree to which the areas of postsynaptic membrane covered by the neurotransmitter released in response to successive action potentials overlap. This, in turn, depends on the area of postsynaptic membrane covered by single synaptic vesicles (sometimes referred to, simply, as the "postsynaptic area"), the detailed morphology of the endplate, the quantal parameters, and the kinetics of vesicle-pool cycling. Thus, this frequency might be different for different species, and even for different muscle fibers of the same species.

The issue of the size of the postsynaptic area has been addressed in the past in the context of both the neuromuscular junction (Hartzell et al., 1975) and neuron–neuron synapses (Trussell et al., 1993; Otis et al., 1996; Barbour and Häusser, 1997; Tureček and Trussell, 2000; Chen et al., 2002; Pugh and Raman, 2005), and is key to any treatment of short-term depression of postsynaptic origin. The extent to which these areas overlap, however,

has remained elusive in the case of the vertebrate endplate. In the snake neuromuscular junction, Hartzell et al. (1975) have clearly shown that the postsynaptic areas corresponding to vesicles "recruited" by the same action potential overlap partially if the acetylcholinesterase (AChE) activity is inhibited, but a firm conclusion could not be drawn from their experiments for the situation in which AChE is fully active. Simulation studies addressing this particular issue have subsequently suggested that, under normal conditions (i.e., intact AChE activity), these areas do not overlap at all (Salpeter, 1987), as if the rapid hydrolyzing effect of AChE limited the lateral spread of the released ACh and completely isolated postsynaptic areas from one another. This would maximally reduce the frequency at which any given receptor interacts with ACh during repetitive stimulation. Although this is clearly a possibility, it would be desirable to address this crucial aspect of synaptic transmission directly, with experiments.

In summary, the data presented here support the well-established notion that, in a physiological context, wild-type muscle AChRs are largely unaffected by desensitization (Edmonds et al., 1995). Indeed, it seems that the behavior of this receptor would not be much different if desensitization did not occur at all. This apparent lack of physiological relevance for such a highly conserved functional property of a protein remains most puzzling. More importantly, our results provide compelling evidence that entry into desensitization contributes to the time course of deactivation in gain-of-function mutants of the muscle AChR. This raises the interesting possibility that, at mutant endplates, the availability of activatable receptors decreases along a train of repetitive stimulation. Experiments using approaches that mimic synaptic transmission more closely than the fast perfusion of outside-out patches used here are, undoubtedly, needed.

We thank Jessica Gasser for technical assistance.

This work was supported by National Institutes of Health grant R01 NS042169 to C. Grosman.

Olaf S. Andersen served as editor.

Submitted: 2 May 2006
Accepted: 9 October 2006

REFERENCES

Auerbach, A., and A. Akk. 1998. Desensitization of mouse nicotinic acetylcholine receptor channels. A two-gate mechanism. *J. Gen. Physiol.* 112:181–197.

Barbour, B., and M. Häusser. 1997. Intersynaptic diffusion of neurotransmitter. *Trends Neurosci.* 20:377–384.

Cachelin, A.B., and D. Colquhoun. 1989. Desensitization of the acetylcholine receptor of frog end-plates measured in a vaseline-gap voltage clamp. *J. Physiol.* 415:159–188.

Chen, C., D.M. Blitz, and W.G. Regehr. 2002. Contributions of receptor desensitization and saturation to plasticity at the retinogeniculate synapse. *Neuron.* 33:779–788.

Colquhoun, D., and A.G. Hawkes. 1982. On the stochastic properties of bursts of single ion channel openings and of clusters of bursts. *Philos. Trans. R. Soc. Lond. B Biol. Sci.* 300:1–89.

Colquhoun, D., and A.G. Hawkes. 1995. A Q-matrix cookbook. *In* Single-Channel Recording. B. Sakmann and E. Neher, editors. Plenum Press, New York. 589–633.

Colquhoun, D., A.G. Hawkes, A. Merlushkin, and B. Edmonds. 1997. Properties of single ion channel currents elicited by a pulse of agonist concentration or voltage. *Philos. Trans. R. Soc. Lond. A.* 355:1743–1786.

Dilger, J.P., and Y. Liu. 1992. Desensitization of acetylcholine receptors in BC3H-1 cells. *Pflugers Arch.* 420:479–485.

Dudel, J., M. Schramm, C. Franke, E. Ratner, and H. Parnas. 1999. Block of quantal end-plate currents of mouse muscle by physostigmine and procaine. *J. Neurophysiol.* 81:2386–2397.

Edelstein, S.J., and J.-P. Changeux. 1998. Allosteric transitions of the acetylcholine receptor. *Adv. Protein. Chem.* 51:121–184.

Edmonds, B., A.J. Gibb, and D. Colquhoun. 1995. Mechanisms of activation of muscle nicotinic acetylcholine receptors and the time course of endplate currents. *Annu. Rev. Physiol.* 57:469–493.

Elenes, S., and A. Auerbach. 2002. Desensitization of diliganded mouse muscle nicotinic acetylcholine receptor channels. *J. Physiol.* 541:367–383.

Engel, A.G., K. Ohno, and S.M. Sine. 2003. Congenital myasthenic syndromes: progress over the past decade. *Muscle Nerve.* 27:4–25.

Franke, C., H. Parnas, G. Hovav, and J. Dudel. 1993. A molecular scheme for the reaction between acetylcholine and nicotinic channels. *Biophys. J.* 64:339–356.

Grosman, C., and A. Auerbach. 2000. Asymmetric and independent contribution of the second transmembrane segment 12' residues to diliganded gating of acetylcholine receptor channels. A single-channel study with choline as the agonist. *J. Gen. Physiol.* 115:637–651.

Grosman, C., and A. Auerbach. 2001. The dissociation of acetylcholine from open nicotinic receptor channels. *Proc. Natl. Acad. Sci. USA.* 98:14102–14107.

Hartzell, H.C., S.W. Kuffler, and D. Yoshikami. 1975. Post-synaptic potentiation: interaction between quanta of acetylcholine at the skeletal neuromuscular synapse. *J. Physiol.* 251:427–463.

Heidmann, T., and J.-P. Changeux. 1980. Interaction of a fluorescent agonist with the membrane-bound acetylcholine receptor from *Torpedo marmorata* in the millisecond time range: resolution of an "intermediate" conformational transition and evidence for positive cooperative effects. *Biochem. Biophys. Res. Commun.* 97:889–896.

Hennig, R., and T. Lømo. 1985. Firing patterns of motor units in normal rats. *Nature.* 314:164–166.

Jackson, M.B., B.S. Wong, C.E. Morris, H. Lecar, and C.N. Christian. 1983. Successive openings of the same acetylcholine receptor channel are correlated in open time. *Biophys. J.* 42:109–114.

Jonas, P. 1995. Fast application of agonists to isolated membrane patches. *In* Single-Channel Recording. B. Sakmann and E. Neher, editors. Plenum Press, New York. 213–243.

Karlin, A. 1967. On the application of "a plausible model" of allosteric proteins to the receptor for acetylcholine. *J. Theor. Biol.* 16:306–320.

Katz, B., and S. Thesleff. 1957. A study of the desensitization produced by acetylcholine at the motor end-plate. *J. Physiol.* 138:63–80.

Land, B.R., E.E. Salpeter, and M.M. Salpeter. 1981. Kinetic parameters for acetylcholine interaction in intact neuromuscular junction. *Proc. Natl. Acad. Sci. USA.* 78:7200–7204.

Magleby, K.L., and C.F. Stevens. 1972. A quantitative description of end-plate currents. *J. Physiol.* 223:173–197.

Magleby, K.L., and B.S. Pallotta. 1981. A study of desensitization of acetylcholine receptors using nerve-released transmitter in the frog. *J. Physiol.* 316:225–250.

Neubig, R.R., and J.B. Cohen. 1980. Permeability control by cholinergic receptors in *Torpedo* postsynaptic membranes: agonist dose–response relations measured at second and millisecond times. *Biochemistry.* 19:2770–2779.

Ohno, K., D.O. Hutchinson, M. Milone, J.M. Brengman, C. Bouzat, S.M. Sine, and A.G. Engel. 1995. Congenital myasthenic syndrome caused by prolonged acetylcholine receptor channel openings due to a mutation in the M2 domain of the epsilon subunit. *Proc. Natl. Acad. Sci. USA.* 92:758–762.

Otis, T., S. Zhang, and L.O. Trussell. 1996. Direct measurement of AMPA receptor desensitization induced by glutamatergic synaptic transmission. *J. Neurosci.* 16:7496–7504.

Pugh, J.R., and I.M. Raman. 2005. $GABA_A$ receptor kinetics in the cerebellar nuclei: evidence for detection of transmitter from distant release sites. *Biophys. J.* 88:1740–1754.

Purohit, Y., and C. Grosman. 2006. Estimating binding affinities of the nicotinic receptor for low-efficacy ligands using mixtures of agonists and two-dimensional concentration–response relationships. *J. Gen. Physiol.* 127:719–735.

Qin, F., A. Auerbach, and F. Sachs. 1996. Estimating single-channel kinetic parameters from idealized patch-clamp data containing missed events. *Biophys. J.* 70:264–280.

Qin, F. 2004. Restoration of single-channel currents using the segmental *k*-means method based on Hidden Markov modeling. *Biophys. J.* 86:1488–1501.

Reitstetter, R., R.J. Lukas, and R. Gruener. 1999. Dependence of nicotinic acetylcholine receptor recovery from desensitization on the duration of agonist exposure. *J. Pharmacol. Exp. Ther.* 289:656–660.

Rothberg, B.S., and K.L. Magleby. 1998. Kinetic structure of large-conductance Ca^{2+}-activated K^+ channels suggests that the gating includes transitions through intermediate or secondary states. A mechanism for flickers. *J. Gen. Physiol.* 111:751–780.

Sakmann, B., J. Patlak, and E. Neher. 1980. Single acetylcholine-activated channels show burst-kinetics in presence of desensitizing concentrations of agonist. *Nature.* 286:71–73.

Salpeter, M.M. 1987. Vertebrate neuromuscular junctions: general morphology, molecular organization, and functional consequences. *In* The Vertebrate Neuromuscular Junction. M.M. Salpeter, editor. Alan R. Liss, Inc., New York. 1–54.

Trussell, L.O., S. Zhang, and I.M. Raman. 1993. Desensitization of AMPA receptors upon multiquantal neurotransmitter release. *Neuron.* 10:1185–1196.

Tureček, R., and L.O. Trussell. 2000. Control of synaptic depression by glutamate transporters. *J. Neurosci.* 20:2054–2063.

Wathey, J.C., M.M. Nass, and H.A. Lester. 1979. Numerical reconstruction of the quantal event at nicotinic synapses. *Biophys. J.* 27:145–164.

Wyllie, D.J.A., P. Béhé, and D. Colquhoun. 1998. Single-channel activations and concentration jumps: comparison of recombinant NR1a/NR2A and NR1a/NR2D NMDA receptors. *J. Physiol.* 510:1–18.